Article

First-Principles Insight into Pd-Doped C_3N Monolayer as a Promising Scavenger for NO, NO_2 and SO_2

Ruochen Peng [1], Qu Zhou [1,*] and Wen Zeng [2,*]

1   College of Engineering and Technology, Southwest University, Chongqing 400715, China; ruochenpeng1207@163.com
2   College of Materials Science and Engineering, Chongqing University, Chongqing 400044, China
*   Correspondence: zhouqu@swu.edu.cn (Q.Z.); wenzeng@cqu.edu.cn (W.Z.); Tel.: +86-130-683-05845 (Q.Z.)

Abstract: The adsorption and sensing behavior of three typical industrial toxic gases NO, NO_2 and SO_2 by the Pd modified C_3N monolayer were studied in this work on the basic first principles theory. Meanwhile, the feasibility of using the Pd doped C_3N monolayer (Pd-C_3N) as a sensor and adsorbent for industrial toxic gases was discussed. First, the binding energies of two doping systems were compared when Pd was doped in the N-vacancy and C-vacancy sites of C_3N to choose the more stable doping structure. The result shows that the doping system is more stable when Pd is doped in the N-vacancy site. Then, on the basis of the more stable doping model, the adsorption process of NO, NO_2 and SO_2 by the Pd-C_3N monolayer was simulated. Observing the three gases adsorption systems, it can be found that the gas molecules are all deformed, the adsorption energy (E_{ad}) and charge transfer (Q_T) of three adsorption systems are relatively large, especially in the NO_2 adsorption system. This result suggests that the adsorption of the three gases on Pd-C_3N belongs to chemisorption. The above conclusions can be further confirmed by subsequent deformable charge density (DCD) and density of state (DOS) analysis. Besides, through analyzing the band structure, the change in electrical conductivity of Pd-C_3N after gas adsorption was studied, and the sensing mechanism of the resistive Pd-C_3N toxic gas sensor was obtained. The favorable adsorption properties and sensing mechanism indicate that the toxic gas sensor and adsorbent prepared by Pd-C_3N have great application potential. Our work may provide some guidance for the application of a new resistive sensor and gas adsorbent Pd-C_3N in the field of toxic gas monitoring and adsorption.

Keywords: Pd-C_3N monolayer; first-principles calculation; toxic gas; adsorption

1. Introduction

Nowadays, with the progress of the economy and the acceleration of industrialization, the problem of industrial waste gases is becoming more and more serious. The industrial production process produces a large number of industrial waste gases, and these waste gases' emission into the air will spread with the flow of the atmosphere, causing great harm to the environment and threatening the physical and mental health of the people [1,2]. NO, NO_2 and SO_2 are several typical toxic industrial waste gases. Hence, finding an effective method of detecting and adsorbing these toxic gases is of great significance to protect our living environment.

Since the typical two-dimensional (2D) material graphene was successfully synthesized, 2D nanomaterial, such as transition metal dihalogen compounds [3–5], silicene [6,7], germanene [8,9], and stannene [10,11], have attracted extensive attention in academia. The excellent properties of these 2D materials make them have broad application prospects in many areas [12–15]. Whereas, the zero-band gap characteristic of graphene limits its application in the nanoelectronics field [16,17]. Thus, researchers began to explore novel two-dimensional graphene-like materials, such as metal nitrides and carbides [18], III-V nitrides [19–21], etc. Among these new graphene-like materials, a planar honeycomb C_3N

monolayer which can be thought of as a 2×2 graphene supercell substituted by two N atoms is emerging [22,23]. C_3N is a semiconductor, and one of its characteristics compared to graphene is its indirect band gap. Owing to the substitution of N atoms, compared with grapheme, the C_3N monolayer has higher chemical activity and carrier mobility as well as better structural stability [24,25]. Therefore, C_3N may have great application potential in gas sensing and adsorption fields [26,27]. Previous studies have shown that intrinsic C_3N is inert to many toxic gases [28]. The adsorption capacity of nanomaterial with transition metal (TM) doping on gas molecules can be significantly improved due to significant electron hybridization between the TM atom and gas molecule [29–31]. Zhu et al. [32] found that the InN monolayer doped with Pd has a good application prospect in detecting and removing toxic gases CO and NO. Ma et al. [33] found that the Au, Pt, Pd and Ni modified MoS_2 monolayers have good sensing performance for CO and NO gases. Therefore, the doping of Pd may enhance the adsorption capacity of C_3N to toxic gases NO, NO_2 and SO_2. However, so far, few research has been executed in the adsorption properties of the TM doped C_3N (TM-C_3N) monolayer for toxic gases such as NO, NO_2 and SO_2.

Based on first principles, the doping behavior of Pd on C_3N and the adsorption properties of Pd-C_3N for NO, NO_2 and SO_2 were studied in this study. Further, to study the adsorption properties and sensing mechanism of Pd-C_3N for three kinds of toxic gases, the E_{ad}, Q_T, DCD, DOS and band structure were analyzed. The results show that NO, NO_2 and SO_2 can be stably adsorbed by Pd-C_3N, which can be recognized as chemisorption. The adsorption properties and sensing mechanism of Pd-C_3N for toxic gases obtained in this work provide a theoretical basis for further study of the toxic gas resistive sensor and adsorbent prepared by Pd-C_3N.

2. Computation Methods

All the theoretical calculations on the basic density functional theory (DFT) in this paper were carried out in the dispersion-corrected DMol^3 package [34,35]. The exchange-correlation between electrons was handled by the Perdew–Burke–Ernzerhof (PBE) function under the generalized gradient approximation (GGA) to better describe the non-uniform electron density of the system which was closer to the experimental situation [36–38]. The DFT-D method, which was customized by Grimme, was used to understand van der Waals force and long-range interactions better [39]. We used DFT semi-core pseudopotential (DSSP) to handle the effects of core electron relativity and chose double numerical plus polarization (DNP) to calculate the density function of each model [40–42]. In terms of the setup of Monkhorst-Pack k-point mesh, $7 \times 7 \times 1$ was set for geometric optimization and $10 \times 10 \times 1$ for the calculation of static electronic structure [43]. The energy tolerance accuracy, maximum force, and displacement were severally set as 10^{-5} Ha, 0.002 Ha/Å and 0.005 Å [44].

A $2 \times 2 \times 1$ C_3N supercell with 28 C atoms and 13 N atoms was built. In order to prevent the adjacent layers from interacting with each other, the vacuum region was set to 15 Å [45]. The lattice constant of the fully optimized C_3N monolayer was calculated as 4.92 Å, which was basically consistent with the previous report (4.9 Å [46]). The Hirshfeld method was adopted to study the electronic behavior of atoms and molecules [47]. Meanwhile, charge transfer (Q_T) is defined to describe the electronic behavior of Pd doping and gas adsorption systems. A positive Q_T value means the analyte acts as an electron donator, on the contrary, a negative Q_T value means that the analyte acts as an electron acceptor [48].

3. Results and Discussions

3.1. Isolated Gas Molecules and Pd-C_3N Monolayer

Figure 1 displays the optimized structural models of the intrinsic C_3N monolayer and three gas molecules NO, NO_2 and SO_2. At the same time, Table 1 lists the geometrical parameters of the optimized three kinds of gas molecular configurations and Table 2 lists the single atom charges of gas molecules in the gas phase.
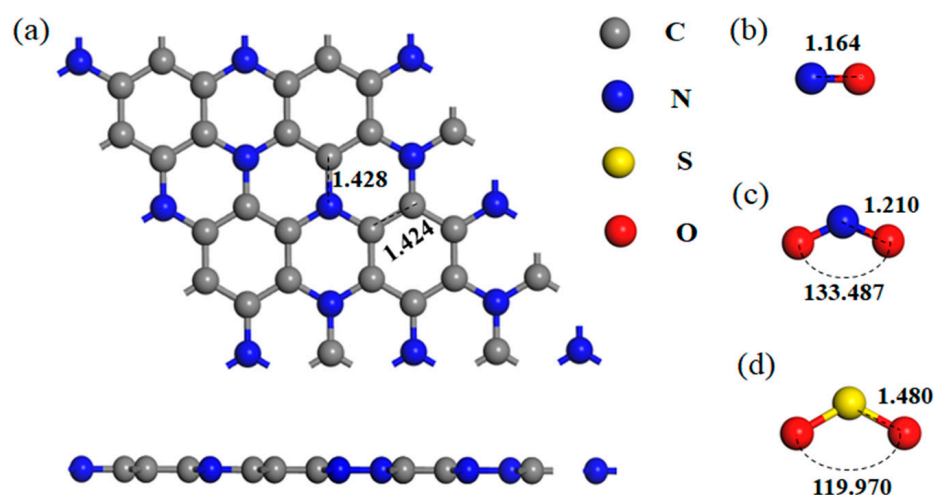
Figure 1. Optimized configuration of (**a**) C_3N monolayer, (**b**) NO, (**c**) NO_2 and (**d**) SO_2.

Table 1. Geometrical parameters of NO, NO_2 and SO_2.

Gas	Bond Length (Å)		Bond Angle (°)	
NO	N-O	1.164	-	-
NO_2	N-O	1.210	O-N-O	133.487
SO_2	S-O	1.480	O-S-O	119.970

Table 2. Single atom charges of gas molecules in the gas phase.

Gas	N	O	S
NO	0.035	−0.035	-
NO_2	0.375	−0.188	-
SO_2	-	0.454	−0.227

According to previous report, the metal atom can be stably adsorbed by the C_3N monolayer with one C atom or one N atom deficiency (simplified as VC-C_3N and VN-C_3N below) due to the strong electrostatic attraction where electronic localization occurs [49]. Therefore, to obtain the most stable doping structure, priority was given to the Pd atom doping at the C-vacancy or N-vacancy site on the C_3N monolayer. The two optimized doping configurations are shown in Figure 2. When Pd is doped at the C-vacancy site, the length of Pd-C and Pd-N is significantly different, which are 1.979 and 2.518 Å, respectively. However, when Pd is doped at the N-vacancy site, the three Pd-C bonds have basically the same length, 2.004, 2.006 and 2.008 Å, respectively. This result shows that the doping system with Pd doping at the N-vacancy site has better central symmetry. In this paper, the stability of the doping system is evaluated by binding energy (E_b), and the calculation formula is as follows:

$$E_b = E_{Pd-C_3N} - E_{vacancy-C_3N} - E_{Pd} \qquad (1)$$

In the above formula, E_{Pd-C_3N} denotes the energy of the Pd-doped system, and $E_{vacancy-C_3N}$ and E_{Pd} denote the energy of the defective C_3N and Pd atom, respectively. The binding energies of Pd doping at the C-vacancy site and N-vacancy site are −4.080 and −5.023 eV, respectively. This result indicates that Pd tends to be doped at the N-vacancy site, because the doping system at this time is more stable.

To further study the electronic behavior of Pd-C_3N, we calculated DCD and DOS, as displayed in Figures 2 and 3, respectively. In the DCD of Figure 2, the areas with increased charge density are shown in red, while the areas with decreased charge density are shown in blue. As shown in Figure 2b, in the doping system where Pd doped is in the N-vacancy site, the charge density around Pd and C atoms decreases, while the charge density around N atoms increases. This result implies the electron-losing property of the Pd atom. In other

words, the Pd atom transfers electrons to the VN-C$_3$N monolayer. Meanwhile, the electron density between the Pd atom and C atom is very high, which suggests that a stable chemical bond in Pd-C is formed, so Pd can be stably adsorbed by VN-C$_3$N. As can be seen from the total DOS of Pd-C$_3$N, the spin up and spin down curves are highly symmetrical. This phenomenon shows that the doping system is not magnetic. Besides, the doping of Pd induces several impurity states, leading to some new peaks of total DOS after doping in the vicinity of −5.5, −4.0, 0.2, 1.0 and 2.0 eV. New peaks can be observed at the top of the valence band and at the bottom of the conduction band, indicating that Pd doping contributes greatly to the states near the Fermi energy. According to Figure 3b, huge hybridization occurs between Pd 4d orbital and C 2p orbital at multiple energy levels, such as −5.5, −2.7, −2 and 0.2 eV. This phenomenon confirms the previous conclusion that Pd can form a stable chemical bond with C and can be stably adsorbed by VN-C$_3$N. Through the analysis of DCD and DOS, it can be concluded that the electronic behavior of VN-C$_3$N has a significant change after doping with the Pd atom.
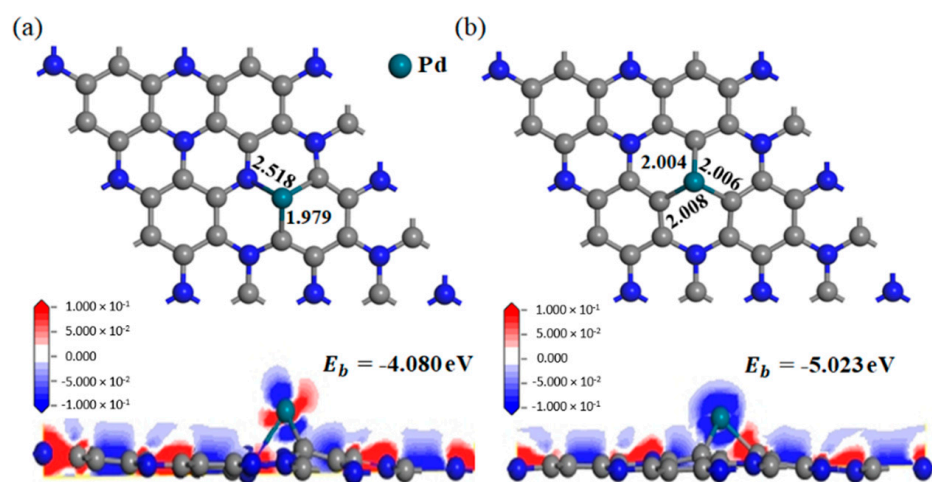

Figure 2. Top view of the optimized structure, side view of DCD (**a**) Pd doped in VC-C$_3$N, (**b**) Pd doped in VN-C$_3$N.
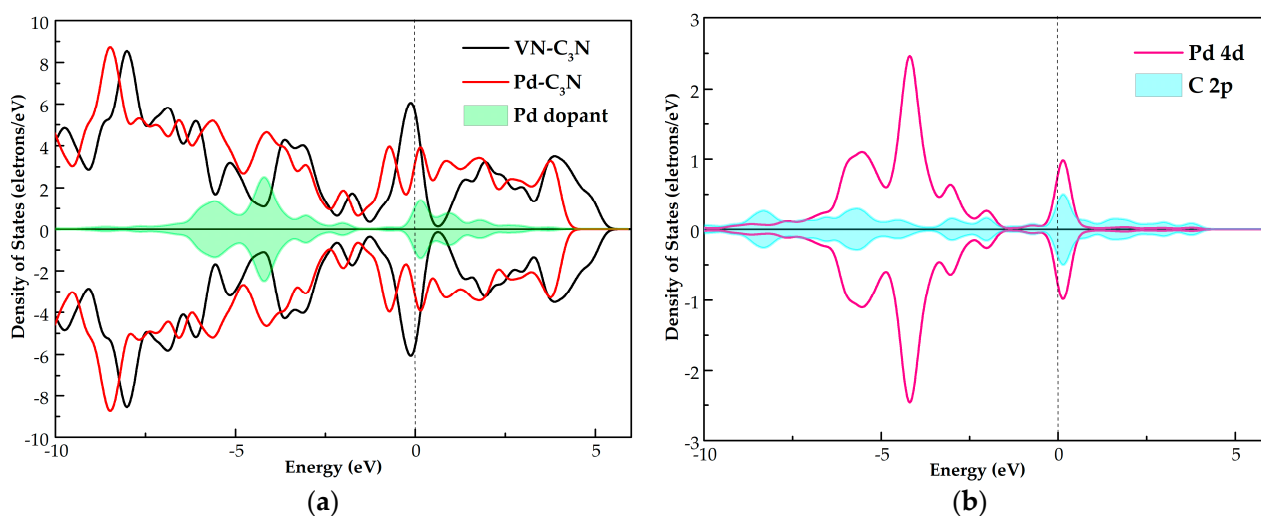

Figure 3. (**a**) TDOS of the VN-C$_3$N monolayer, Pd-C$_3$N monolayer, (**b**) PDOS of the Pd-C$_3$N monolayer, the dotted line indicates the Fermi energy.

3.2. Adsorption Analysis of Pd-C$_3$N Monolayer to NO, NO$_2$, SO$_2$

In order to fully compare various possible configurations of the three gas adsorption systems and find the most stable one for analysis, NO, NO$_2$ and SO$_2$ were placed in different directions on top of the Pd-C$_3$N monolayer. Adsorption energy (E_{ad}) can describe the energy change of each adsorption structure, so it can be used to assess the stability of the system after adsorption of gas. The calculation formula of E_{ad} is as below:

$$E_{ad} = E_{Pd-C_3N/gas} - E_{Pd-C_3N} - E_{gas} \qquad (2)$$

In the above formula, $E_{Pd-C_3N/gas}$ and E_{Pd-C_3N} respectively represent the energy before and after the adsorption of gas by Pd-C$_3$N, and E_{gas} represents the energy of the isolated gas molecule. The adsorption energies of the three gas adsorption systems are all negative, suggesting that the gas adsorption process of Pd-C$_3$N is accompanied by the release of heat. Choose the structure with the lowest E_{ad}, that is, the most stable configuration for subsequent works (as displayed in Figure 4). To understand the mechanism of charge transfer better, deformed charge density (DCD) is also described in Figure 4. Meanwhile, Tables 3 and 4 show the specific characteristic parameters of the three gas adsorption systems.
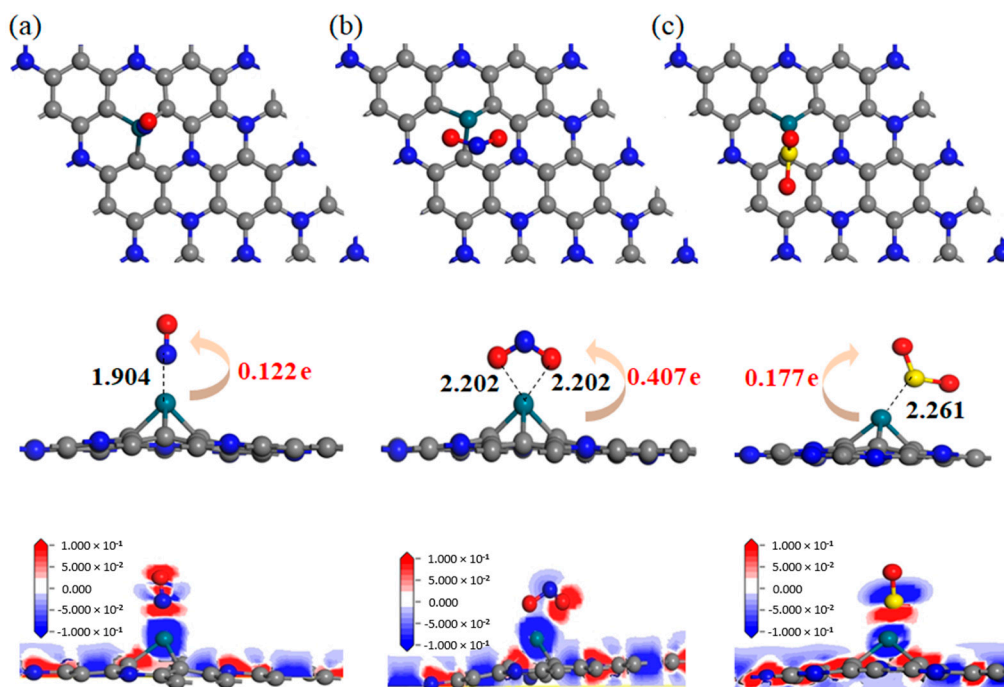

Figure 4. The steadiest adsorption configuration of gas on the Pd-C$_3$N monolayer and the DCD of this configuration (**a**) NO; (**b**) NO$_2$ and (**c**) SO$_2$ adsorption systems.

In the NO adsorption system, the NO molecule is adsorbed on top of the Pd atom and perpendicular to the C$_3$N plane. When NO is adsorbed, the N-O bond elongates from 1.164 to 1.188 Å, indicating that the NO molecule has certain activity during the adsorption process. The E_{ad} of the NO adsorption system is −1.83 eV, so the adsorption of NO by the Pd-C$_3$N monolayer can be identified as chemisorption. Meanwhile, according to the DCD in Figure 4a, the charge density near N atoms and O atoms increases. From the molecular point of view, NO has a 0.122 e negative charge, indicating the electron-receiving property of NO. During the interaction with the Pd-C$_3$N monolayer, NO obtains 0.122 e from it. According to Figure 4b,c, NO$_2$ and SO$_2$ tend to be adsorbed on one side of the Pd dopant in the Pd-C$_3$N monolayer rather than on the top. In addition, the adsorbed NO$_2$ and SO$_2$ molecules are negatively charged, which means that they both act as electron acceptors to absorb 0.407 e and 0.177 e from the Pd-C$_3$N monolayer, respectively. In the NO$_2$ adsorption

system, the N-O bond elongates to 1.281 Å compared to the 1.210 Å in the isolated phase. At the same time, the O-N-O bond angle of the NO_2 molecule in the adsorption system decreases from 133.487° in the gas phase to 111.674°. This significant deformation indicates that NO_2 has obvious geometric activation during its interaction with the Pd dopant. Besides, the charge density near the N atom in the NO_2 adsorption system decreases, while the charge density near the O atom increases. In addition, the E_{ad} of the NO_2 adsorption system is −2.74 eV, which indicates that NO_2 has an ideal chemisorption on the surface of Pd-C_3N, which is supported by large Q_T (−0.407 e) and geometric deformation. In the SO_2 adsorption system, the S-O bond elongates from 1.480 to 1.495 Å, while the O-S-O bond angle decreases from 119.970° to 119.932°, suggesting that SO_2 is activated when interacting with the surface of Pd-C_3N. The E_{ad} of the SO_2 adsorption system is −1.61 eV, Q_T is −0.177 e, which can be used to identify the adsorption as chemisorption.

Table 3. The geometrical parameters of three gas adsorption systems.

System	The Length of Bond (Å)		Bond Angle (°)		Adsorption Distance (Å)
Pd-C_3N + NO	N-O	1.188	-		1.904
	Pd-C	2.046, 2.046, 2.050			
Pd-C_3N + NO_2	N-O	1.281	O-N-O	111.674	2.202
	Pd-C	1.978, 1.979, 2.016			
Pd-C_3N + SO_2	S-O	1.495	O-S-O	119.932	2.261
	Pd-C	2.046, 2.044, 1.990			

Table 4. The characteristic parameters of three gas adsorption systems.

System	Atom	Mulliken Charge (e)	Q_T (e)	E_{ad} (eV)
Pd-C_3N + NO	N	−0.033	−0.122	−1.83
	O	−0.089		
Pd-C_3N + NO_2	N	0.270	−0.407	−2.74
	O_1	−0.338		
	O_2	−0.339		
Pd-C_3N + SO_2	S	0.457	−0.177	−1.61
	O_1	−0.303		
	O_2	−0.331		

Previous reports have shown that E_{ad} of the intrinsic C_3N monolayer adsorption system for NO, NO_2 and SO_2 is −0.248, −0.840 and −0.584 eV, respectively [28]. Comparing to the results in this study, it can be found that the adsorption capacity of Pd-C_3N for NO, NO_2 and SO_2 was significantly higher than that of intrinsic C_3N. At the same time, the adsorption process of three kinds of gas molecules by the Pd-C_3N monolayer is accompanied by a relatively large charge transfer, which indicates that the adsorption of gas will lead to the redistribution of electrons in the whole system and change the electronic behavior of Pd-C_3N. To further explore the electronic behavior of Pd-C_3N during the adsorption of NO, NO_2 and SO_2, DOS is analyzed in the following.

3.3. DOS Analysis of NO, NO_2 and SO_2 Adsorption Systems

DOS is an important parameter for studying the electronic behavior of the interaction between gas and the Pd-C_3N surface. According to Figure 5, the total DOS (TDOS) of the three adsorption systems shift to the right in different degrees compared with the Pd-C_3N monolayer, and some new peaks appear nearby the Fermi level. In the TDOS of

NO adsorption system, novel peaks appear in the vicinity of -1, -0.1 and 2 eV, while in NO_2 and SO_2 adsorption systems, the new peaks appear in the vicinity of -1.5, -0.3 and 0.3 eV. Besides, there are multiple activated states in the gas molecules due to the interaction between it and the surface of the Pd dopant. Then, the orbital hybridization of these activated states with Pd 4d results in new peaks in the TDOS of the three adsorption systems. In particular, the activated states of gas molecules lead to a certain degree of deformation of the states at the top of the conduction band and the bottom of the valence band, which indicates that the adsorption of gas will affect the electronic behavior of Pd-C_3N.
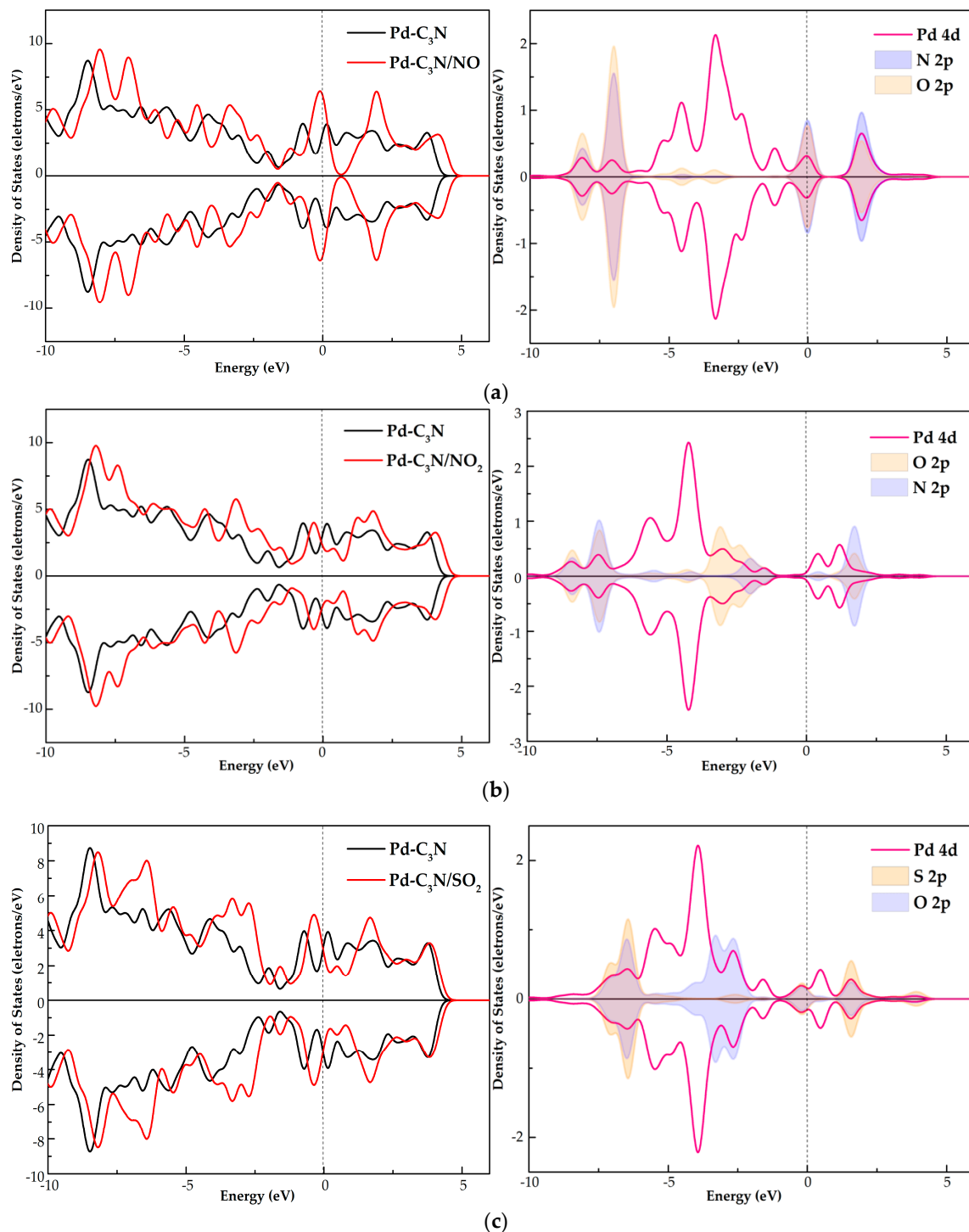

Figure 5. TDOS and PDOS of (**a**) NO, (**b**) NO_2 and (**c**) SO_2 adsorption systems, the dotted line indicates the Fermi energy.

Atomic DOS (PDOS) is shown in Figure 5. In the NO adsorption system, the N 2p and O 2p orbitals of activated NO have certain hybridization with Pd 4d orbitals at -8, -7, 0 (Fermi level) and 2.2 eV. According to the atomic DOS of the NO_2 adsorption system, the Pd 4d orbital is strongly hybridized with N 2p and O 2p orbitals around -8, -7.2 and 2 eV, resulting in a relatively large charge transfer between NO_2 and Pd-C_3N. In the atomic DOS of SO_2 adsorption system, S 2p, O 2p and Pd 4d orbital have strong hybridization at energy levels of -6.3, -2.5, -0.2 and 2 eV, indicating that there is a good orbital interaction between SO_2 and Pd dopant. The strong hybridization between the atomic orbitals of the three gas molecules and Pd 4d orbital again confirms that NO, NO_2 and SO_2 can be stably adsorbed by Pd-C_3N.

In summary, the strong interaction between three gases and Pd-C_3N during gas adsorption process significantly affects the electronic behavior of Pd-C_3N.

3.4. Band Structure Analysis of NO, NO_2 and SO_2 Systems

To further study the change in electrical conductivity of Pd-C_3N after adsorbing gas, we calculated and analyzed the band structure of three adsorption systems (Figure 6). In the band structure, the energy interval with zero energy state density between the conduction band and the valence band is called the band gap [50,51]. The narrower the band gap, the more easily the electron can be excited across the band gap, the higher the conductivity. According to Figure 6a, the band gap of the Pd-C_3N monolayer is 0.203 eV, which is much narrower than that of C_3N (0.44 eV [52]). Besides, the band structure of the doping system does not have an impurity state beyond the Fermi level. Thus, C_3N doped with the Pd atom still has semiconductor property. In the band structure of NO and SO_2 adsorption systems (Figure 6b,d), the new impurity level surpassing the Fermi energy appears at the top of the valence band, causing a zero band gap for both systems. Therefore, the adsorption of NO and SO_2 can be deemed to strong p-type doping for Pd-C_3N [53]. According to Figure 6, the band gap of NO and SO_2 adsorption system is 0 eV, while that of NO_2 adsorption system is 0.091 eV. It can be seen that the band gaps of these three adsorption systems are much narrower than that of Pd-C_3N. This result shows that the conductivity of Pd-C_3N is observably improved after adsorbing gas, especially after adsorbing NO and SO_2. Through calculating and analyzing the band structure of the three adsorption systems, it is helpful to further understand the sensing mechanism of the resistive chemical sensor prepared by Pd-C_3N.
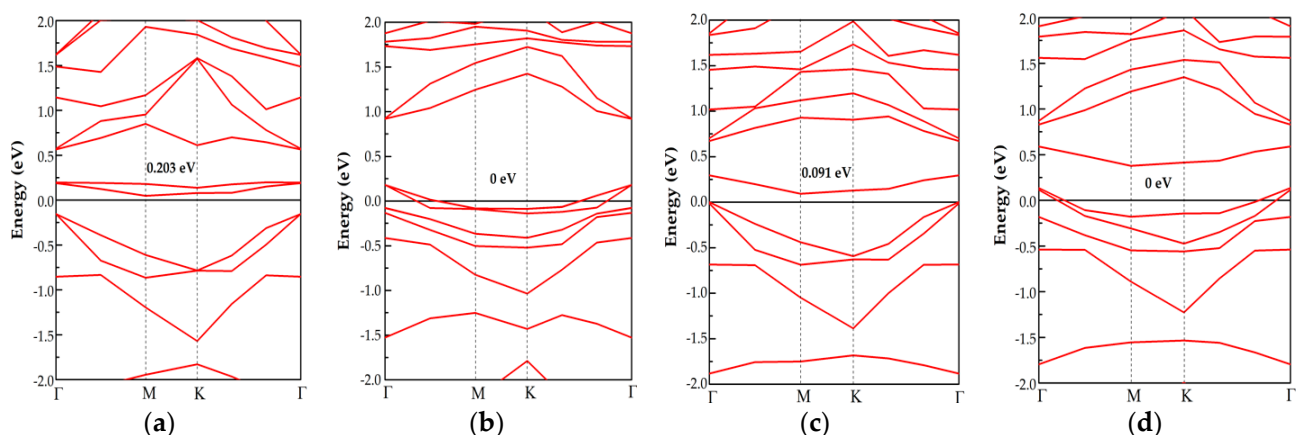

Figure 6. Energy band structure of (**a**) Pd-C_3N monolayer and (**b**) Pd-C_3N/NO, (**c**) Pd-C_3N/NO_2, (**d**) Pd-C_3N/SO_2 systems.

4. Conclusions

The adsorption performance and sensing mechanism of the Pd-C_3N monolayer for three kinds of industrial toxic gases NO, NO_2 and SO_2 were explored based on first principles. The DCD, DOS and band structure were considered to study the change in

electronic behavior and conductivity of Pd-C_3N after adsorbing gas. The main conclusions of this study are listed as below:

1. The Pd dopant is more likely to be adsorbed on the N-vacancy site of the C_3N than the C-vacancy site, because the lower binding energy (E_b = −5.023 eV) of this doping system implies a more stable structure.
2. NO, NO_2 and SO_2 can be stably adsorbed by the Pd-C_3N monolayer and the adsorption can be identified as chemisorption. Besides, the adsorption energy (E_{ad}) of the Pd-C_3N/gas system is much higher than that of the C_3N/gas system. Among three gas adsorption systems, E_{ad} and Q_T of the NO_2 system are the largest, which indicates that Pd-C_3N has the strongest adsorption performance for NO_2.
3. Through the analysis of DOS, it is found that the gas molecules are activated during the interaction with the Pd dopant surface. The orbital hybridization of these activated states with Pd 4d give rise to new peaks in the TDOS of the three adsorption systems, which influences the electronic behavior of Pd-C_3N.
4. Through analyzing the band structure, it can be discovered that the band gap of Pd-C_3N becomes narrower after adsorbing NO, NO_2 and SO_2, which significantly improves the conductivity of Pd-C_3N, especially after adsorbing NO and SO_2.

To sum up, the calculation in this paper can offer some theoretical basis for the further study of Pd-C_3N as a resistive sensor and gas adsorbent for the monitoring and adsorption of typical industrial toxic gases in the environment.

Author Contributions: Conceptualization, R.P.; methodology, R.P. and Q.Z.; validation, R.P. and Q.Z.; investigation, R.P.; resources, Q.Z.; data curation, R.P.; writing—original draft preparation review and editing, R.P.; writing—review and editing, R.P., Q.Z. and W.Z.; visualization, R.P.; supervision, Q.Z.; project administration, Q.Z. and W.Z. All authors have read and agreed to the published version of the manuscript.

Institutional Review Board Statement: Not applicable.

Informed Consent Statement: Not applicable.

Data Availability Statement: The data is available on the request from corresponding author.

Conflicts of Interest: The authors declare no conflict of interest.

References

1. Louw, I. Potential radiological impact of the phosphate industry in South Africa on the public and the environment (Paper 1). *J. Environ. Radioact.* **2020**, *217*, 106214. [CrossRef] [PubMed]
2. Rybicka, E.H. Impact of mining and metallurgical industries on the environment in Poland. *Appl. Geochem.* **1996**, *11*, 3–9. [CrossRef]
3. Li, B.L.; Zhou, Q.; Peng, R.C.; Liao, Y.M.; Zeng, W. Adsorption of SF_6 decomposition gases (H_2S, SO_2, SOF_2 and SO_2F_2) on Sc-doped MoS_2 surface: A DFT study. *Appl. Surf. Sci.* **2021**, *549*, 149271. [CrossRef]
4. Zhang, Y.; Chang, T.R.; Zhou, B.; Cui, Y.T.; Yan, H.; Liu, Z.K.; Schmitt, F.; Lee, J.; Moore, R.; Chen, Y.L.; et al. Direct observation of the transition from indirect to direct bandgap in atomically thin epitaxial $MoSe_2$. *Nat. Nanotechnol.* **2014**, *9*, 111–115. [CrossRef] [PubMed]
5. Huang, X.; Zeng, Z.Y.; Zhang, H. Metal dichalcogenide nanosheets: Preparation, properties and applications. *Chem. Soc. Rev.* **2013**, *42*, 1934–1946. [CrossRef] [PubMed]
6. Hu, W.; Xia, N.; Wu, X.J.; Li, Z.Y.; Yang, J.L. Silicene as a highly sensitive molecule sensor for NH_3, NO and NO_2. *Phys. Chem. Chem. Phys.* **2014**, *16*, 6957–6962. [CrossRef]
7. Hu, W.; Wu, X.J.; Li, Z.Y.; Yang, J.L. Helium separation via porous silicene based ultimate membrane. *Nanoscale* **2013**, *5*, 9062–9066. [CrossRef] [PubMed]
8. Xia, W.Q.; Hu, W.; Li, Z.Y.; Yang, J.L. A first-principles study of gas adsorption on germanene. *Phys. Chem. Chem. Phys.* **2014**, *16*, 22495–22498. [CrossRef]
9. Kaloni, T.P. Tuning the structural, electronic, and magnetic properties of germanene by the adsorption of 3d transition metal atoms. *J. Phys. Chem. C* **2014**, *118*, 25200–25208. [CrossRef]

10. Yan, Z.Q.; Tao, C.; Bai, Y.; Liu, S.P. Adsorption of nitrogen based gas molecules on noble metal functionalized carbon nitride nanosheets: A theoretical investigation. *Comput. Theor. Chem.* **2021**, *1194*, 112950. [CrossRef]

11. Nagarajan, V.; Chandiramouli, R. Adsorption behavior of NH_3 and NO_2 molecules on stanene and stanane nanosheets—A density functional theory study. *Chem. Phys. Lett.* **2018**, *695*, 162–169. [CrossRef]

12. Pierucci, D.; Zribi, J.; Henck, H.; Chaste, J.; Silly, M.G.; Bertran, F.; Le Fèvre, P.; Gil, B.; Summerfield, A.; Beton, P.H.; et al. Van der Waals epitaxy of two-dimensional single-layer h-BN on graphite by molecular beam epitaxy: Electronic properties and band structure. *Appl. Phys. Lett.* **2018**, *112*, 253102. [CrossRef]

13. Zhou, Q.; Zeng, W.; Chen, W.G.; Xu, L.N.; Kumar, R.; Umar, A. High sensitive and low-concentration sulfur dioxide (SO_2) gas sensor application of heterostructure NiO-ZnO nanodisks. *Sens. Actuators B Chem.* **2019**, *298*, 126870. [CrossRef]

14. Comini, E.; Baratto, C.; Faglia, G.; Ferroni, M.; Vomiero, A.; Sberveglieri, G. Quasi-one dimensional metal oxide semiconductors: Preparation, characterization and application as chemical sensors. *Prog. Mater. Sci.* **2009**, *54*, 1–67. [CrossRef]

15. Zhou, Q.; Umar, A.; Sodki, E.; Amine, A.; Xu, L.N.; Gui, Y.G.; Ibrahim, A.A.; Kumar, R.; Baskoutas, S. Fabrication and characterization of highly sensitive and selective sensors based on porous NiO nanodisks. *Sens. Actuators B Chem.* **2018**, *259*, 604–615. [CrossRef]

16. Novoselov, K.S.; Geim, A.K.; Morozov, S.V.; Jiang, D.; Katsnelson, M.I.; Grigorieva, I.V.; Dubonos, S.V.; Firsov, A.A. Two-dimensional gas of massless Dirac fermions in grapheme. *Nature* **2005**, *438*, 197–200. [CrossRef] [PubMed]

17. Sprinkle, M.; Siegel, D.; Hu, Y.; Hicks, J.; Tejeda, A.; Taleb-Ibrahimi, A.; Le Fevre, P.; Bertran, F.; Vizzini, S.; Enrique, H.; et al. First direct observation of a nearly ideal graphene band structure. *Phys. Rev. Lett.* **2009**, *103*, 226803. [CrossRef]

18. Naguib, M.; Mochalin, V.N.; Barsoum, M.W.; Gogotsi, Y. 25th anniversary article: MXenes: A new family of two-dimensional materials. *Adv. Mater.* **2014**, *26*, 992–1005. [CrossRef] [PubMed]

19. Cui, H.; Zhang, X.X.; Li, Y.; Chen, D.C.; Zhang, Y. First-principles insight into Ni-doped InN monolayer as a noxious gases scavenger. *Appl. Surf. Sci.* **2019**, *494*, 859–866. [CrossRef]

20. Cui, H.; Liu, T.; Zhang, Y.; Zhang, X.X. Ru-InN monolayer as a gas scavenger to guard the operation status of SF_6 insulation devices: A first-principles theory. *IEEE Sens. J.* **2019**, *19*, 5249–5255. [CrossRef]

21. Sajjad, M.; Feng, P. Study the gas sensing properties of boron nitride nanosheets. *Mater. Res. Bull.* **2014**, *49*, 35–38. [CrossRef]

22. Ma, D.W.; Zhang, J.; Tang, Y.A.; Fu, Z.M.; Yang, Z.X.; Lu, Z.S. Repairing single and double atomic vacancies in a C_3N monolayer with CO or NO molecules: A first-principles study. *Phys. Chem. Chem. Phys.* **2018**, *20*, 13517–13527. [CrossRef] [PubMed]

23. Qian, C.X.; Sun, W.; Hung, D.L.H.; Qiu, C.Y.; Makaremi, M.; Kumar, S.G.H.; Wan, L.L.; Ghoussoub, M.; Wood, T.E.; Xia, M.K.; et al. Catalytic CO_2 reduction by palladium-decorated silicon–hydride nanosheets. *Nat. Catal.* **2019**, *2*, 46–54. [CrossRef]

24. Cui, H.P.; Zheng, K.; Zhang, Y.Y.; Ye, H.Y.; Chen, X.P. Superior selectivity and sensitivity of C_3N sensor in probing toxic gases NO_2 and SO_2. *IEEE Electron Device Lett.* **2018**, *39*, 284–287. [CrossRef]

25. Ma, D.W.; Zhang, J.; Li, X.X.; He, C.Z.; Lu, Z.W.; Lu, Z.S.; Yang, Z.X.; Wang, Y.X. C_3N monolayer as promising candidates for NO_2 sensors. *Sens. Actuator B Chem.* **2018**, *266*, 664–673. [CrossRef]

26. Babar, V.; Sharma, S.; Schwingenschlogl, U. Highly sensitive sensing of NO and NO_2 gases by monolayer C_3N. *Adv. Theory Simul.* **2018**, *1*, 1700008. [CrossRef]

27. Eslami, M.; Moradi, M.; Moradi, R. DFT investigation of hydrogen adsorption on the C_3N nanotube. *Vacuum* **2016**, *133*, 7–12. [CrossRef]

28. Xiong, H.H.; Zhang, H.H.; Gan, L. A new bifunctional C_3N nanosheet of NO_2, SO_2 gas sensor and CO_2 separation: A first-principles study. *Phys. E* **2021**, *126*, 114463. [CrossRef]

29. Zhou, Q.; Xu, L.N.; Umar, A.; Chen, W.G.; Kumar, R. Pt nanoparticles decorated SnO_2 nanoneedles for efficient CO gas sensing applications. *Sens. Actuators B Chem.* **2018**, *256*, 656–664. [CrossRef]

30. Cui, H.; Chen, D.C.; Zhang, Y.; Zhang, X.X. Dissolved gas analysis in transformer oil using Pd catalyst decorated $MoSe_2$ monolayer: A first-principles theory. *Sustain. Mater. Technol.* **2019**, *20*, e00094. [CrossRef]

31. Liao, Y.M.; Peng, R.C.; Peng, S.D.; Zeng, W.; Zhou, Q. The adsorption of H_2 and C_2H_2 on Ge-doped and Cr-doped graphene structures: A DFT study. *Nanomaterial* **2021**, *11*, 231. [CrossRef]

32. Zhu, S.Y.; Ma, S.X. Adsorption and sensing behaviors of Pd-doped InN monolayer upon CO and NO molecules: A first-principles study. *Appl. Sci.* **2019**, *9*, 3390. [CrossRef]

33. Ma, D.W.; Ju, W.W.; Li, T.X.; Zhang, X.W.; He, C.Z.; Ma, B.Y.; Lu, Z.S.; Yang, Z.X. The adsorption of CO and NO on the MoS_2 monolayer doped with Au, Pt, Pd, or Ni: A first-principles study. *Appl. Surf. Sci.* **2016**, *383*, 98–105. [CrossRef]

34. Capelle, K.; Gross, E.K.U. Spin-density functionals from current-density functional theory and vice versa: A road towards new approximations. *Phys. Rev. Lett.* **1997**, *78*, 1872–1875. [CrossRef]

35. Gao, X.; Zhou, Q.; Wang, J.X.; Xu, L.N.; Zeng, W. DFT Study on the Selective Adsorption Properties of Modified Graphene for SF_6 Decompositions. *IEEE Sens. J.* **2021**, *21*, 3193–3200. [CrossRef]

36. Zhang, Y.X.; Zeng, W.; Ye, H.; Li, Y.Q. Enhanced carbon monoxide sensing properties of TiO_2 with exposed (001) facet: A combined first-principle and experimental study. *Appl. Surf. Sci.* **2018**, *442*, 507–516. [CrossRef]

37. Zhang, Y.X.; Zeng, W.; Li, Y.Q. Computational study of surface orientation effect of rutile TiO_2 on H_2S and CO sensing mechanism. *Appl. Surf. Sci.* **2019**, *495*, 143619. [CrossRef]

38. Gao, X.; Zhou, Q.; Wang, J.X.; Xu, L.N.; Zeng, W. Performance of intrinsic and modified graphene for the adsorption of H_2S and CH_4: A DFT study. *Nanomaterial* **2020**, *10*, 299. [CrossRef]

39. Tkatchenko, A.; Distasio, R.A.; Head-Gordon, M.; Scheffler, M. Dispersion-corrected Moller-Plesset second-order perturbation theory. *J. Chem. Phys.* **2009**, *131*, 094106. [CrossRef] [PubMed]

40. Chen, D.C.; Zhang, X.X.; Tang, J.; Cui, H.; Li, Y. Noble metal (Pt or Au)-doped monolayer MoS_2 as a promising adsorbent and gas-sensing material to SO_2, SOF_2 and SO_2F_2: A DFT study. *Appl. Phys. A Mater. Sci. Process.* **2018**, *124*, 194. [CrossRef]

41. Gui, X.X.; Zhou, Q.; Peng, S.D.; Xu, L.N.; Zeng, W. Dissolved gas analysis in transformer oil using Sb-doped graphene: A DFT study. *Appl. Surf. Sci.* **2020**, *533*, 147509. [CrossRef]

42. Wang, Y.H.; Li, D.Y.; Lai, X.B.; Liu, B.Y.; Chen, Y.B.; Wang, F.P.; Wang, R.M.; Zhang, L.W. Direct observation of the hysteretic Fermi level modulation in monolayer MoS_2 field effect transistors. *Curr. Appl. Phys.* **2020**, *20*, 293–303. [CrossRef]

43. Monkhorst, H.J.; Pack, J.D. Special points for Brillouin-zone integrations. *Phys. Rev. B* **1976**, *13*, 5188–5192. [CrossRef]

44. Cui, H.; Zhang, X.X.; Zhang, J.; Tang, J. Adsorption behaviour of SF_6 decomposed species onto Pd_4-decorated single-walled CNT: A DFT study. *Mol. Phys.* **2018**, *116*, 1749–1755. [CrossRef]

45. Wu, P.; Yin, N.Q.; Li, P.; Cheng, W.J.; Huang, M. The adsorption and diffusion behavior of noble metal adatoms (Pd, Pt, Cu, Ag and Au) on a MoS_2 monolayer: A first-principles study. *Phys. Chem. Chem. Phys.* **2017**, *19*, 20713–20722. [CrossRef]

46. Makaremi, M.; Mortazavi, B.; Singh, C.V. Adsorption of metallic, metalloidic, and nonmetallic adatoms on two-dimensional C_3N. *J. Phys. Chem. C* **2017**, *121*, 18575–18583. [CrossRef]

47. Hirshfeld, F.L. Bonded-atom fragments for describing molecular charge densities. *Theor. Chim. Acta* **1977**, *44*, 129–138. [CrossRef]

48. Liu, D.K.; Gui, Y.G.; Ji, C.; Tang, C.; Zhou, Q.; Li, J.; Zhang, X.X. Adsorption of SF_6 decomposition components over Pd (1 1 1): A density functional theory study. *Appl. Surf. Sci.* **2019**, *465*, 172–179. [CrossRef]

49. Lu, Z.S.; Yang, M.X.; Ma, D.W.; Lv, P.; Li, S.; Yang, Z.X. CO oxidation on $Mn-N_4$ porphyrin-like carbon nanotube: A DFT-D study. *Appl. Surf. Sci.* **2017**, *426*, 1232–1240. [CrossRef]

50. Cui, H.; Zhang, X.X.; Chen, D.C.; Tang, J. Pt & Pd decorated CNT as a workable media for SOF_2 sensing: A DFT study. *Appl. Surf. Sci.* **2018**, *471*, 335–341.

51. Cui, H.; Zhang, X.X.; Zhang, G.Z.; Tang, J. Pd-doped MoS_2 monolayer: A promising candidate for DGA in transformer oil based on DFT method. *Appl. Surf. Sci.* **2019**, *470*, 1035–1042. [CrossRef]

52. Zhou, X.D.; Feng, W.X.; Guan, S.; Fu, B.T.; Su, W.Y.; Yao, Y.G. Computational characterization of monolayer C_3N: A two-dimensional nitrogen-graphene crystal. *J. Mater. Res.* **2017**, *32*, 2993–3001. [CrossRef]

53. Ma, D.W.; Wang, Q.G.; Li, T.X.; He, C.Z.; Ma, B.Y.; Tang, Y.A.; Lu, Z.S.; Yang, Z.X. Repairing sulfur vacancies in the MoS_2 monolayer by using CO, NO and NO_2 molecules. *J. Mater. Chem. C* **2016**, *4*, 7093–7101. [CrossRef]